JACS
JOURNAL OF THE AMERICAN CHEMICAL SOCIETY
Article
pubs.acs.org/JACS

Evidence of σ- and π-Dimerization in a Series of Phenalenyls

Zhongyu Mou,[†] Kazuyuki Uchida,[‡] Takashi Kubo,*[,‡] and Miklos Kertesz*[,†]

[†]Department of Chemistry, Georgetown University, Washington, D.C. 20057, United States
[‡]Department of Chemistry, Graduate School of Science, Osaka University, Toyonaka, Osaka 560-0043, Japan

Supporting Information

ABSTRACT: Phenalenyl and a wide variety of its derivatives form stable radicals, which often associate in various aggregates with interesting properties that include magnetism and high electrical conductivity. The two main modes of aggregation involve π-stacking pancake multicenter bond formation and σ-bond formation. We explore the energetics of the various σ- and π-dimers for six phenalenyl derivatives with both computational and experimental methods. A modern density functional theory (M05-2X) is used to survey the potential energy surface revealing the mechanism of the aggregation. In order to enrich experimental data, the triphenyl and trimethyl derivatives are newly prepared and their aggregation behaviors are investigated by various analytical methods including ESR, ^{1}H NMR, UV−vis, and single-crystal X-ray diffraction. The agreement between computations and experiments are very good forming the basis of describing trends in this series. We find that π-dimer formation can proceed via an asynchronous concerted path from the monomers or in a stepwise process via σ-dimers. The strength of the π-stacking pancake interaction depends strongly on substituents and covers a wide range both in terms of binding energies and contact distances. The spin densities in the π-stacking dimers reflect these trends and display a wide range of diradicaloid characters. Many σ-dimer configurations compete some of which are separated by small barriers leading to fluxional structures between σ-bonded configurations or σ- and π-bonded configurations.

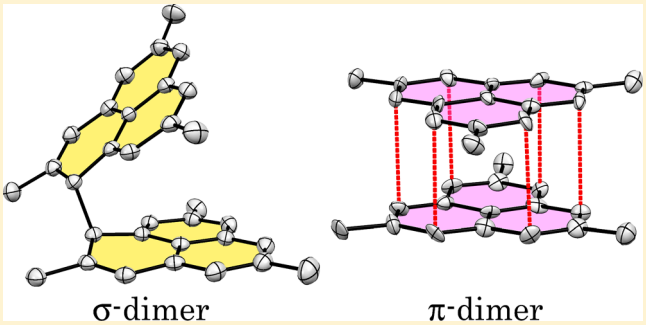

INTRODUCTION

Phenalenyl (**1**, Scheme 1) is a stable odd-alternant hydrocarbon π-radical which has been studied for its electronic and magnetic properties.[1] This stable neutral radical has gained importance in organic chemistry as a fundamental building block for organic conducting materials.[2] Dimerization of phenalenyl and its derivatives has recently attracted attention due to a unique two-electron, 12-center (2e/12c) π−π stacking bonding interaction between two phenalenyl monomers.[3,4] This type of π−π stacking bonding has been called pancake bonding,[5] which is the result of a singlet diradicaloid state where two electrons from the multicenter SOMO orbitals of the radical monomers form bonding combinations across the inter-radical space. This results in closer distances as well as stronger than van der Waals bonding interactions.[6] The stabilization of the π stacking configuration by virtue of pancake bonding makes it competitive energetically with σ-bonding. The main subject of this work is to provide detailed computations on the relative energies of six σ- and π-bonded radical dimers derived from the prototypical phenalenyl system, including two newly synthesized and characterized derivatives.

Previous experimental studies on phenalenyl have shown that both σ-dimers and π-dimers can be formed.[7,8] The fact that $\mathbf{1}_2$ σ-dimer and $\mathbf{1}_2$ π-dimer are close in energy may result in some interesting properties such as fluxional bonding.[9] We present the first systematic study of energetically competitive conformations of six dimerized phenalenyl derivatives:

Scheme 1. Monomer Radical of Phenalenyl and Its Radical Derivatives Discussed in This Paper[a]

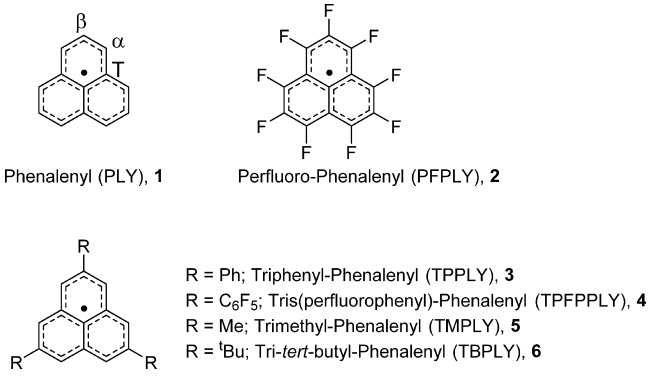

Phenalenyl (PLY), **1**

Perfluoro-Phenalenyl (PFPLY), **2**

R = Ph; Triphenyl-Phenalenyl (TPPLY), **3**
R = C_6F_5; Tris(perfluorophenyl)-Phenalenyl (TPFPPLY), **4**
R = Me; Trimethyl-Phenalenyl (TMPLY), **5**
R = ^{t}Bu; Tri-*tert*-butyl-Phenalenyl (TBPLY), **6**

[a]T indicates the tertiary carbon close to the α-carbon.

phenalenyl (PLY), perfluoro-phenalenyl (PFPLY), triphenyl-phenalenyl (TPPLY), tris(perfluorophenyl)-phenalenyl (TPFPPLY), trimethyl-phenalenyl (TMPLY), and tri-*tert*-butyl-phenalenyl (TBPLY) (**2**−**6**, Scheme 1). We combined available experimental data with calculations in order to interpret the characteristics of the dimers. The analysis provides

Received: September 7, 2014
Published: November 13, 2014

   dx.doi.org/10.1021/ja509243p | J. Am. Chem. Soc. 2014, 136, 18009−18022

insights into tautomerization reactions of these related phenalenyl dimers shedding light on the relative roles of σ-bonding, pancake-bonding, and van der Waals (vdW) interactions. Because so far the only phenalenyls isolated are **1**, **4**, and **6**, we add new experimental data on the synthesis and experimental characterization of **3** and **5**. Combination of various experimental methods including electron spin resonance (ESR), ^{1}H NMR, and UV−vis spectroscopy and X-ray crystallographic measurements fully support the computational results.

Two main conformations of the π-dimer are the eclipsed and the staggered, both providing perfect $\pi-\pi$ overlap[10] of the SOMO orbitals for all compounds discussed here. Scheme 2 illustrates the SOMO orbital for **1** and the bonding and antibonding combination of the two SOMO orbitals in the pancake bonded staggered π-dimer of $\mathbf{1}_2$, which represents a strongly attractive interaction preferring maximum overlap. However, even without the various β-substitutions that are present from **2**−**6**, for the parent $\mathbf{1}_2$ the staggered configuration is significantly more stable than the eclipsed.[11]

Scheme 2. Illustration of Bonding (HOMO) and Antibonding (LUMO) Combinations of Two SOMOs in the $\mathbf{1}_2$ π-Dimer at the UM052X/6-31G(d) Level, Along with the Orbital Interaction Diagram (Right) and the SOMO of the Monomer (Bottom)[a]

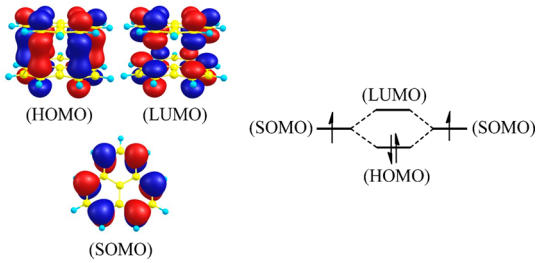

[a]Note the multicenter nature of the bonding interaction in the HOMO of the dimer.

The configurational space for the σ-dimers is more complex. We adopted the notation introduced in ref 8 for various $\mathbf{1}_2$ σ-isomers (Chart 1). Two basic types of σ-dimerizations arise: the *RR* (staggered) and the *RS* (eclipsed). Within each type further configurations can be identified,[8] and their relative energetics is one of the main subjects in this work.

METHODS

Experimental Methods. Synthesis of a hydro-precursor of **3** was accomplished in seven steps from 2,7-diphenylnaphthalene. Detailed synthetic procedures and product characterization are summarized in the Supporting Information. A hydro-precursor of **5** was prepared according to the literature by Leitch et al.[12] Generation of **3** and **5** were carried out in toluene/hexane or dichloromethane/hexane mixed solvents in a sealed degassed tube by the dehydrogenation of the hydro-precursors with *p*-chloranil, giving rise to dark violet cubic crystals of the $\mathbf{3}_2$ π-dimer and colorless platelet crystals of the $\mathbf{5}_2$ σ-dimer. Single crystals of the $\mathbf{5}_2$ π-dimer were obtained by melting the powder of the $\mathbf{5}_2$ σ-dimer at 573 K in a sealed degassed tube and subsequently cooling to room temperature. Single-crystal X-ray diffraction (XRD) analysis was performed on a Rigaku/Varimax diffractometer (Mo Kα, λ = 0.71069 Å). Variable-temperature ESR measurements of **3** and **5** were carried out in degassed toluene on a JEOL JES-RE1X spectrometer. Variable-temperature ^{1}H NMR spectra of **3** in degassed CD_2Cl_2 were measured on a JEOL ECS400 spectrometer. UV−vis absorption spectra of **3** and **6** were measured in KBr pellets with a JASCO V-570 spectrometer.

Chart 1. Newman Projections for Six $\mathbf{1}_2$ σ-Isomers[8] and Illustration of $\mathbf{1}_2$(*RS*1)[a]

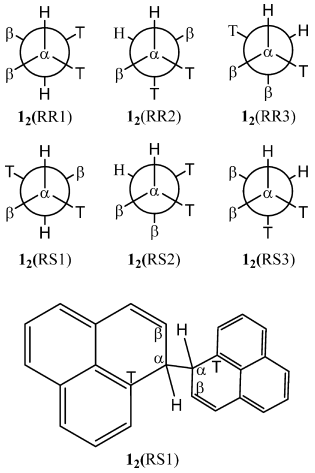

[a]The Newman projection is along the σ-bond connecting two α-carbons on a σ-dimer of a phenalenyl or its derivative.

Computational Methods. We employed density functional theory (DFT) applying an M05-class meta-generalized gradient approximation (GGA) density functional for this study.[13] We chose this method because it is a well-established DFT including dispersion effects and previous studies showed good results for phenalenyl-related dimerization geometries and energetics.[14,15] The broken-symmetry spin-unrestricted method was adopted for all open-shell species, i.e., π dimers and monomers, and was labeled by the prefix (U). There is no broken-symmetry spin-unrestricted solution for the σ-bonded dimers. Unless stated otherwise, all geometry optimizations as well as vibrational frequency calculations were done for the monomers and dimers with (U)M05-2X/6-31G(d) for PLY and (U)M05-2X/6-31G(d,p) for PFPLY, TMPLY, TPPLY, and TPFPPLY. We adopted (U)M05-2X/6-31G(d) for PLY because the addition of the p set on H has a negligible effect, as shown in Table S1. The interaction energy (E_{int}) was obtained by taking the difference of the total energy, E_{tot}, between dimer complex and the sum of two monomers.

$$E_{int}(\text{before ZPE}) = E_{tot}(\text{dimer}) - 2E_{tot}(\text{monomer}) \quad (1)$$

Energy barriers corresponding to a particular transition structure, TS, are given as the smaller of two values along the torsional scans, as

$$\Delta E_{TS} = E_{TS} - E_{total}(\text{closest higher local minimum}) \quad (2)$$

The zero-point energy (ZPE) correction, E_{int}(ZPE corr), was computed as

$$E_{int}(\text{after ZPE}) = E_{int}(\text{before ZPE}) + E_{ZPE}(\text{dimer}) - 2E_{ZPE}(\text{monomer}) \quad (3)$$

The separation of the total interaction energy into a component due to the SOMO−SOMO binding interaction and the remaining van der Waals term (that includes dispersion, Pauli repulsion, and electrostatic terms) can be symbolically written as

$$E_{tot} = E_{(SOMO-SOMO)} + E_{vdW} \quad (4)$$

Following Mota et al.[16] and extensive validation at a high wave function level,[11,17] we approximate the first term as

$$E_{(SOMO-SOMO)} = E(\text{singlet at min. of singlet}) - E(\text{triplet at min. of singlet}) \quad (5)$$

The potential energy surfaces (PESs) were studied by constrained relaxed scans and rigid scans. For the PES curve regarding bond

dx.doi.org/10.1021/ja509243p | J. Am. Chem. Soc. 2014, 136, 18009−18022

stretching, constrained optimizations (relaxed scans) were performed with one fixed distance of r, where r is the distance between the closest α-carbons (Figure 1). For π-dimers the six r distances were kept equal

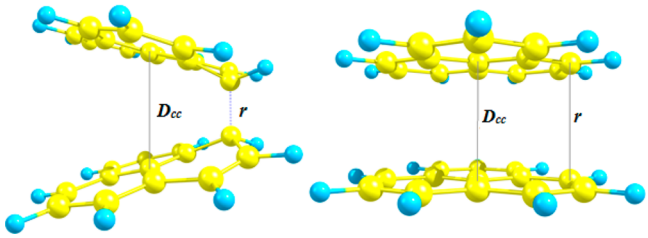

Figure 1. Optimized geometry of $\mathbf{1}_2(RR2)$ σ-dimer and the $\mathbf{1}_2$ π-dimer isomer indicating the α-carbon to α-carbon distance, r. For the pancake-bonded $\mathbf{1}_2$ π-dimer, there are six contacts equal to r. D_{cc} is the central C−C distance in the pancake dimer.

when rigid scans were performed. Relaxed torsional PES scans were obtained by performing constrained optimizations as a function of the dihedral angle θ (Figure 2). For optimized π-dimers, the r values shown in the tables are the averages of six α-carbon distances.

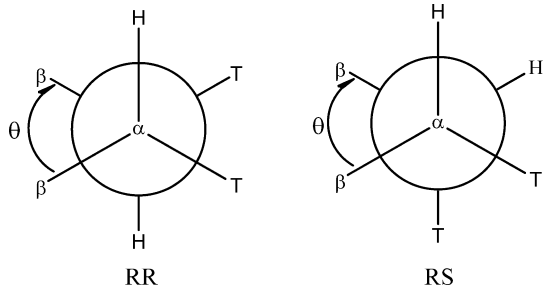

Figure 2. Definition of the torsional angle θ for *RR* and *RS* σ-isomers.

Vibrational frequency analyses were carried out in order to categorize stationary points as minima or transition states and to obtain the zero point energy (ZPE). Frequencies for ZPE were not scaled. All minima, except where noted otherwise, were confirmed obtaining all real vibrational frequencies, all transition structures (TSs) were identified by one imaginary frequency at the saddle point. Mulliken population-based spin density was analyzed to characterize the nature of the dimerization. Mulliken spin density presented in this study is the total spin density of one monomer. All quantum mechanical computations were performed with the Gaussian09 package (D.01).[18] Visualization was done by ChemCraft.[19]

RESULT AND DISCUSSION

Phenalenyl (PLY). Small et al. computed the relative energies of the six $\mathbf{1}_2$ σ-isomers shown in Chart 1 using MP2/6-31G(d).[8] We analyzed the torsional potential energy surfaces and identified the transition structures. $\mathbf{1}_2(RS2)$ and $\mathbf{1}_2(RS3)$ are energetically equivalent because they are enantiomers so we only presented $\mathbf{1}_2(RS2)$ in this study. Five optimized $\mathbf{1}_2$ σ-dimer configurations are shown in Figure 3. Combined with $\mathbf{1}_2\pi$ in Figure 1, six optimized $\mathbf{1}_2$-dimers are presented. We calculated the interaction energy of these dimers and the results are shown in Table 1.

Comparing with the MP2 calculation,[8] the UM05-2X energies are reasonably close and hence we proceed with UM05-2X calculations in the rest of this work. According to Table 1, the interaction energy for all $\mathbf{1}_2$ σ-dimers are similar and they are 4−6 kcal/mol lower than the $\mathbf{1}_2$ π-dimer. However, ZPE correction narrows the energy difference to only 0.6−3.0 kcal/mol. The ZPE corrections for $\mathbf{1}_2$ σ-dimers are almost identical due to the same bonding type (σ-bond). The ZPE correction for the $\mathbf{1}_2$ π-dimer is significantly smaller than for $\mathbf{1}_2$ σ-dimers because of the loss of a σ-bond. It is worth noting that the σ-bond distance, r, is longer than normal σ-bonds because of steric repulsions between the two phenalenyl monomers but still shorter than in extreme cases such as hexaphenylethane.[20]

The small computed energy differences among these configurations may indicate fluxional bonding, depending on the barrier between them.[14,21] To study this conformational isomerism we present rotational scans along the σ-bonds for each of the $\mathbf{1}_2$ σ-dimers as well as bond stretching scans between $\mathbf{1}_2$ π-dimer and one of the $\mathbf{1}_2$ σ-dimers. The torsional energy scans for the *RR* (staggered) and the *RS* (eclipsed) configurations as a function of dihedral angle θ, are presented in Figure 4.

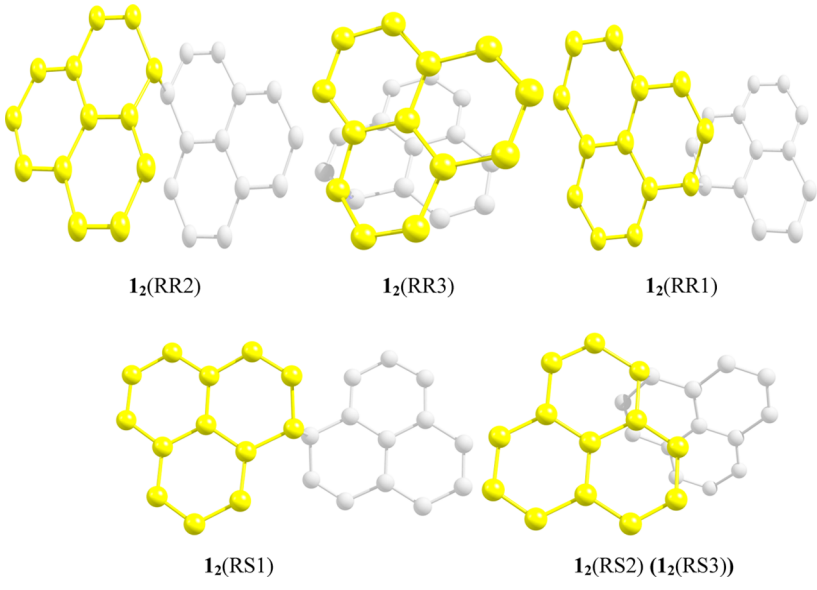

Figure 3. Optimized geometries of $\mathbf{1}_2$ σ-dimers. Hydrogen atoms are omitted for clarity.

dx.doi.org/10.1021/ja509243p | J. Am. Chem. Soc. 2014, 136, 18009−18022

Table 1. Interaction Energies, E_{int}, and Selected Distances of the Optimized 1_2-Dimers Using (U)M05-2X/6-31G(d)[a]

	$1_2(RR1)$	$1_2(RR2)$	$1_2(RR3)$	$1_2(RS1)$	$1_2(RS2)$	$1_2\pi$
E_{int} from ref 8[b]	−14.50	−13.10	−15.30	−13.50	−15.30	NA
E_{int}(before ZPE)	−14.55	−14.39	−16.65	−13.67	−16.15	−10.71
E_{int}(ZPE corr)	3.75	3.59	3.86	3.79	3.60	1.47
E_{int}(after ZPE)	−10.81	−10.78	−12.79	−9.88	−12.55	−9.24
symmetry	C_2	C_2	C_2	S_2	none	D_{3h}
α-carbon distance (r)	1.605	1.610	1.582	1.597	1.586	3.084
D_{cc}[c]	3.137					
spin density[d]	0	0	0	0	0	0.642

[a] E_{int} values are in kcal/mol, and distances are in Å. [b] MP2/6-31G(d) calculation from ref 8 before any correction. [c] Central carbon−carbon distance. [d] Sum of Mulliken spin density of a monomer in the dimer.

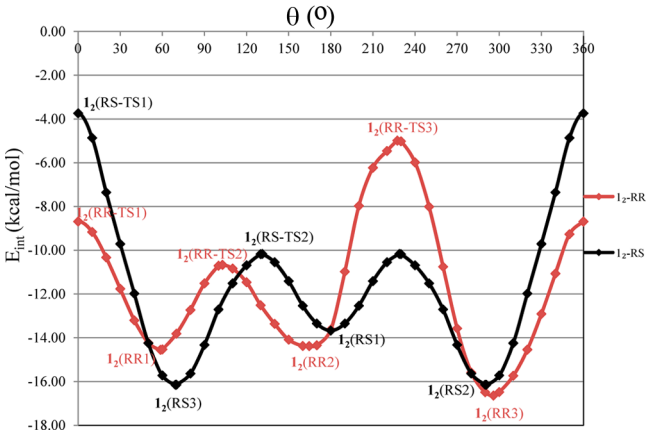

Figure 4. Relaxed torsional energy scan as a function of θ around the σ-bond for 1_2-*RR* and 1_2-*RS*. Energy calculated at the UM052X/6-31G(d) level. For the notation of the different local minima, see Figure 3. Various transition structures are indicated by TS.

Figure 4 shows three local minima for each of the two scans. The 1_2-*RS* scan shows symmetry because $1_2(RS2)$ and $1_2(RS3)$ are enantiomers. Both curves have three local minima and correspondingly three barriers. Tables 2 and 3 show the stationary points on the rotational scans of Figure 4. The 1_2-*RS* scan which corresponds to the black line in Figure 4 shows a lower barrier at 131.2° and a higher barrier at 0°. The lower energy barrier at 131.2° (and 228.8° by symmetry) would be the one through which the isomerization between $1_2(RS1)$ and $1_2(RS2)$ (or $1_2(RS3)$) would proceed.

Table 2. Interaction Energies, E_{int}, and Energy Barriers, ΔE_{TS}, for Stationary Points along the 1_2-*RS* Scan[a]

	$1_2(RS3)$	$1_2(RS1)$	$1_2(RS\text{-}TS2)$	$1_2(RS\text{-}TS1)$
E_{int}	−16.65	−13.67	−10.17	−3.74
ΔE_{TS}			3.50	9.93

[a] All energies are without ZPE correction, calculated at the UM052X/6-31G(d) level, and given in kcal/mol. See eqs 1 and 2.

Table 3. Interaction Energies, E_{int}, and Energy Barriers, ΔE_{TS}, for Stationary Points along the 1_2-*RR* Scan[a]

	$1_2(RR1)$	$1_2(RR2)$	$1_2(RR3)$	$1_2(RR\text{-}TS1)$	$1_2(RR\text{-}TS2)$	$1_2(RR\text{-}TS3)$
E_{int}	−14.55	−14.39	−16.65	−8.70	−10.67	−4.7
ΔE_{TS}				5.85	3.71	9.68

[a] All energies are without ZPE correction, calculated at the M052X/6-31G(d) level, and given in kcal/mol. See eqs 1 and 2.

There are six stationary points with three local minima and three TSs on the rotational scan of 1_2-*RR* scan, as shown in Table 3, corresponding to the red line in Figure 4. Two out of the three TSs, $1_2(RR\text{-}TS1)$ and $1_2(RR\text{-}TS2)$, represent more accessible pathways. The study of the pathway is important to explore the possibility to form the 1_2 π-dimer from the presented calculation results imply that we might be able to detect the presence of 1_2 π-dimer experimentally. The $1_2(RR2)$ is the closest configuration that can transform into $1_2\pi$, and we present data on this scan as a function of distance r in Figure 5

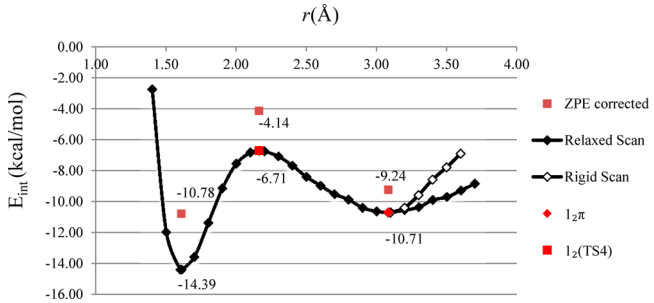

Figure 5. E_{int} scan between $1_2(RR2)$ and $1_2\pi$ at the UM052X/6-31G(d) level. 1_2(TS4) is the transition structure along the bond-stretching path of 1_2.

Table 4. Energies and Selected Distances for Stationary Points on the $1_2(RR2)$−$1_2\pi$ Scan[a]

	$1_2(RR2)$	1_2(TS4)	$1_2\pi$
E_{int}(before ZPE)	−14.39	−6.71	−10.71
E_{int}(ZPE corr)	3.61	2.57	1.47
E_{int}(after ZPE)	−10.78	−4.14	−9.24
r	1.610	2.164	3.084
ΔE_{TS}		5.10	

[a] Energy values are in kcal/mol and distances are in Å.

and Table 4. The TS along the dissociation path is denoted as 1_2(TS4). It is important to realize that the dissociation of the π-dimer, $1_2\pi$, proceeds without a barrier, and therefore the π-dimer can form spontaneously from the monomer independent from temperature.

The two minima in Figure 5 correspond to $1_2(RR2)$ and $1_2\pi$ separated by a stationary point, 1_2(TS4), that is 5.10 kcal/mol higher in energy than $1_2\pi$ after ZPE correction. The α-carbon distance of 1_2(TS4) is at r = 2.164 Å corresponding to a typical TS value for breaking a σ-bond.[14] An interesting separation

dx.doi.org/10.1021/ja509243p | J. Am. Chem. Soc. 2014, 136, 18009−18022

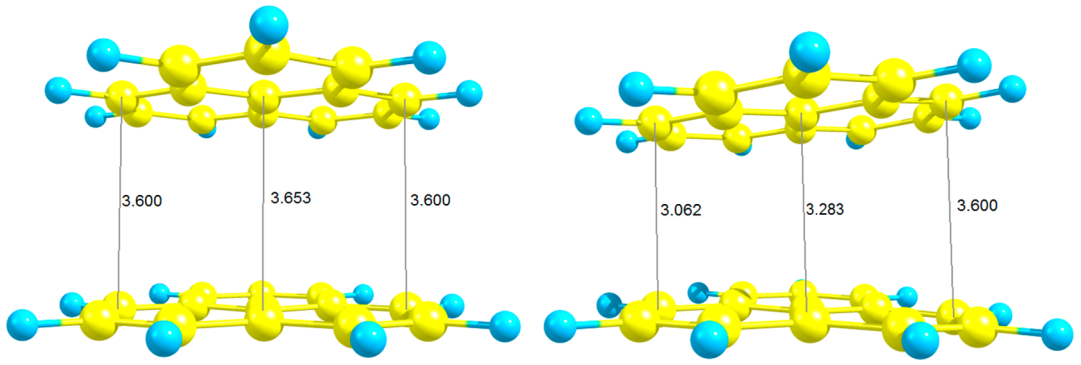

Figure 6. Single-point structure on the rigid scan (left) vs optimized structure on the relaxed scan (right) at r = 3.6 Å along the bond-stretching scan in Figure 5 for $\mathbf{1}_2$.

occurs between the rigid scan and relaxed scan in the r > 3.0 Å regime in Figure 5 (empty vs full diamonds) which is a consequence of the multicenter nature of pancake bonding: while breaking one of the six $\alpha-\alpha$ contacts, the other five break at a lower rate in the relaxed scan. Figure 6 shows the geometries corresponding to the two scans at an intermediate separation of r = 3.6 Å, indicating that the reverse reaction, the formation of the π-stacking dimer, is asynchronous.

The diradical character of the 2e/mc bonding is one of the unusual characteristics of pancake bonding which is reflected in the spin density. Figure 7 shows the spin density based on the Mulliken population analysis along the reaction pathway between $\mathbf{1}_2(RR2)$ and $\mathbf{1}_2\pi$.

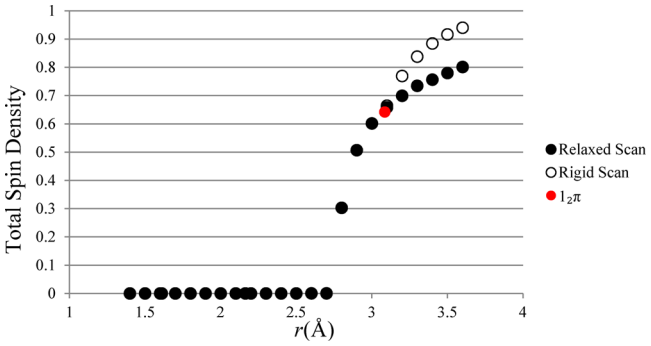

Figure 7. Total spin density of a **1** monomer in the $\mathbf{1}_2$ dimer along the $\mathbf{1}_2(RR2)$ to $\mathbf{1}_2\pi$ scan using UM052X/6-31G(d). The Coulson–Fischer point is at r = 2.7 Å.

The Coulson–Fischer (bifurcation) point is at r = 2.7 Å. It also indicates that the electronic structure of $\mathbf{1}_2$(TS4) (r = 2.164 Å) is closer to that of the σ-bonded $\mathbf{1}_2(RR2)$ tautomer and therefore it does not exhibit pancake bonding. According to the HOMO–LUMO orbital diagram for $\mathbf{1}_2\pi$ (Scheme 2), $\pi-\pi$ interactions solely occur at α-carbon positions. A split from r = 3.1Å between relaxed scan and rigid scan corresponds well with Figure 5. There is no particular reason for the spin density of α-carbon approaching ~0.35 in Figure S1; however, the limiting value of 1 in Figure 7 for total spin density of a monomer is consistent with the separation into two uncoupled radicals.

Perfluoro-Phenalenyl (PFPLY). The preparation and characterization of the perfluoro-phenalenyl (**2**) and its dimers have not yet been reported. Below is the summary of our results on modeling its various dimers in analogy to the parent **1** system. Table 5 summarizes the computed energetics of the isomers and a few key bond distance data.

The results in Table 5 indicate that the $\mathbf{2}_2$ σ-dimers behave similarly to the $\mathbf{1}_2$ σ-dimers: they are close in energy to one another and also have similar ZPE energies. However, the interaction energy of the $\mathbf{2}_2$ σ-dimers is much lower than for the $\mathbf{1}_2$ σ-dimers. This can be rationalized by referring to the difference of the bond dissociation energy between F_3C-CF_3 and H_3C-CH_3 bond. According to previous studies,[22] the CC bond in F_3C-CF_3 is about ~9 kcal/mol stronger than in H_3C-CH_3. In our case, although σ-bond environments are not exactly the same, it does explain the major source of the interaction energy difference between the $\mathbf{1}_2$ and $\mathbf{2}_2$ σ-dimers. While all $\mathbf{2}_2$ σ-dimers are very close in energy, their torsional scans along the σ-bond,presented in Figure S2, show a number of local barriers somewhat different from the analogous scans of the $\mathbf{1}_2$ σ-dimers. Table 5 shows that E_{int} difference between $\mathbf{2}_2(RR2)$ and $\mathbf{2}_2\pi$ is 10.11 kcal/mol before ZPE correction and 7.70 kcal/mol after correction. This large difference in E_{int} indicates that the $\mathbf{2}_2$ σ-dimers would be preferred over the $\mathbf{2}_2$ π-dimer.

The σ-bonded dimers are significantly more stable for the $\mathbf{2}_2$ case, and thus the computations suggest that the π-dimer is

Table 5. Interaction Energies, E_{int}, and Selected Distances of the Optimized $\mathbf{2}_2$-Dimers Using (U)M05-2X/6-31G(d,p)[a]

	$\mathbf{2}_2(RR1)$	$\mathbf{2}_2(RR2)$	$\mathbf{2}_2(RR3)$	$\mathbf{2}_2(RS1)$	$\mathbf{2}_2(RS2)$	$\mathbf{2}_2\pi$
E_{int}(before ZPE)	−26.72	−25.41	−26.24	−25.67	−25.80	−15.30
E_{int}(ZPE corr)	4.50	4.34	4.20	4.33	4.31	1.93
E_{int}(after ZPE)	−22.22	−21.07	−22.04	−21.34	−21.49	−13.37
symmetry	C_2	C_2	C_2	S_2	none	D_{3h}
r	1.593	1.590	1.576	1.583	1.579	2.933
D_{cc}						3.109
spin density[b]	0	0	0	0	0	0.702

[a] E_{int} values are in kcal/mol and distances are in Å. [b] Sum of Mulliken spin density of a monomer in the dimer.

dx.doi.org/10.1021/ja509243p | J. Am. Chem. Soc. 2014, 136, 18009–18022

unlikely to be observed for this derivative. Nevertheless a bond stretching scan is of interest in order to explore trends in the relative stabilities of σ-bonded and pancake bonded π-dimers. Figure S3 shows the relaxed and unrelaxed dissociation-scan for $\mathbf{2}_2$ while Table 6 summarizes the energetics of this scan. Similar to the dissociation of $\mathbf{1}_2\pi$, $\mathbf{2}_2\pi$ can also form from the monomers without a barrier.

Table 6. Energy and Distance Comparisons between Stationary Points in the $\mathbf{2}_2(RR2)$–$\mathbf{2}_2\pi$ Scans As Shown in Figure S3[a]

	$\mathbf{2}_2(RR2)$	$\mathbf{2}_2$(TS)	$\mathbf{2}_2\pi$
E_{int}(before ZPE)	−25.41	−11.01	−15.30
E_{int}(ZPE corr)	4.34	3.33	1.93
E_{int}(after ZPE)	−21.07	−7.68	−13.37
r	1.590	2.206	2.933
ΔE_{TS}		5.69	

[a] E_{int} values are in kcal/mol and distances are in Å. $\mathbf{2}_2$(TS) indicates the transition structure on the scan shown in Figure S3.

According to Figure S3, the bond stretching energy scan for $\mathbf{2}_2$ is very similar to that of the parent $\mathbf{1}_2$ shown in Figure 5. The spin density scan also shows a similar trend as presented in Figure S4.

Two differences arise between the spin density scans of $\mathbf{1}_2$ and $\mathbf{2}_2$. The Coulson–Fischer point occurs at a smaller r value in $\mathbf{2}_2$ (2.5 vs 2.7 Å), and the α-carbons' spin density is smaller for $\mathbf{2}_2$. The equilibrium distance for $\mathbf{2}_2\pi$ is shorter, at 2.93 Å, compared to 3.08 Å for $\mathbf{1}_2\pi$, and the perfluoro dimer has larger interaction energy in all configurations compared to the parent $\mathbf{1}_2$. Fluorine acts as an electron-withdrawing group, decreasing the α-carbon electron density. This results in the decrease of spin density as well as increase of E_{int}. This trend corresponds well with our previous study on the effect of various β-position substitutions versus E_{int} on **1**.[14] As far as pancake bonding is concerned in $\mathbf{2}_2\pi$, all factors (shorter and stronger bond, stronger electron pairing due to a lower spin density) indicate a stronger pancake bond for $\mathbf{2}_2\pi$ compared to $\mathbf{1}_2\pi$ if it could be observed.

Triphenyl-Phenalenyl (TPPLY). Tri-*tert*-butyl-phenalenyl (TBPLY, **6**) and its dimer have been synthesized and studied.[1,14,23] It is believed that TBPLY will only form $\mathbf{6}_2$ π-dimer because of steric repulsion effect on possible $\mathbf{6}_2$ σ-dimers. We will return to TBPLY but first we study the dimerization of the β-substituted triphenyl-phenalenyl (TPPLY, **3**). Following the σ-dimerization of **1** and **2**, there could possibly be similar $\mathbf{3}_2$ σ-dimers with low energy if side group steric repulsion could be properly avoided. We have obtained five $\mathbf{3}_2$ σ-dimers as well as two $\mathbf{3}_2$ π-dimers in our energy minimizations. These are represented in Figure 8, their energetics are shown in Table 7. The discussion of the experimental data follows the analysis of the potential energy surface.

Large differences in E_{int} occur between some of the $\mathbf{3}_2$ σ-dimers as shown in Table 7. Unlike $\mathbf{1}_2$ and $\mathbf{2}_2$ dimers, the potential energy surface of the $\mathbf{3}_2$-dimers is more complicated because of the phenyl torsions, phenyl–phenyl interactions and phenyl–phenalenyl interactions. The most stable $\mathbf{3}_2$ σ-dimer is $\mathbf{3}_2(RR2)$, the structure of which is closest to $\mathbf{3}_2\pi$. This indicates that the closed structures (more phenyl–phenyl and phenalenyl–phenalenyl interaction) such as $\mathbf{3}_2(RR2)$ as well as $\mathbf{3}_2(RS2)$ are more stable than the open structures. $\mathbf{3}_2(RR2)$ is the lowest in E_{int}, and it appears that the edge-to-face vdW

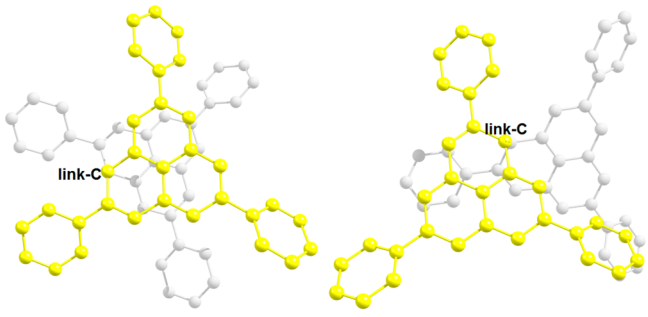

$\mathbf{3}_2$(RR2) $\mathbf{3}_2$(RS2)

Figure 8. Top view of two most stable optimized $\mathbf{3}_2$ σ-dimer geometries. (H atoms are hidden). Gray and yellow indicate the two monomers connected by a σ-bond. Link-C indicates the linking carbons. The other three are given in Figure S5.

phenyl–phenyl attraction[24] and vdW attraction between central phenalenyls contribute significantly to the stability of this structure. Note that a certain amount of steric repulsion is unavoidable in these crowded σ-bonded dimers as also indicated by the stretched lengths of these bonds at about 1.6 Å. The second most stable σ-bonded structure, $\mathbf{3}_2(RS2)$, has neither phenyl–phenyl interactions nor central phenalenyl–phenalenyl interactions, so it is energetically slightly higher than $\mathbf{3}_2(RR2)$. The third most stable structure is $\mathbf{3}_2(RR3)$, which is about 2 kcal/mol higher than $\mathbf{3}_2(RS2)$ and 4–6 kcal/mol lower than $\mathbf{3}_2(RR1)$ and $\mathbf{3}_2(RS1)$. $\mathbf{3}_2(RR3)$ exhibits no phenyl–phenyl repulsions and has a weak phenyl–phenalenyl attraction. The other two isomers, $\mathbf{3}_2(RR1)$ and $\mathbf{3}_2(RS1)$, exhibit some phenyl–phenyl repulsions between two pairs of phenyl groups and thus are the least stable among the $\mathbf{3}_2$ σ-dimers.

Beside the $\mathbf{3}_2$ σ-dimers, there are two possible $\mathbf{3}_2$ π-dimers: the one with parallel phenyl configuration, which we named as $\mathbf{3}_2$ π-parablade ($\mathbf{3}_2\pi_{PB}$), and the one with edge-to-face phenyl configuration, which we named as $\mathbf{3}_2$ π-antiblade ($\mathbf{3}_2\pi_{AB}$), referring to the phenyls as blades of two propellers facing one another. Figure 9 shows the corresponding optimized geometries.

There are several differences between these two π-dimers. First of all, geometry convergence problems plagued the optimization due to the flatness of the PES and the large number of coupled soft degrees of freedom especially for $\mathbf{3}_2\pi_{PB}$ even after a large number of iterations. We included this structure in our discussion, but only an approximate ZPE value was available. Table 7 shows that $\mathbf{3}_2\pi_{PB}$ is ∼5 kcal/mol less stable than $\mathbf{3}_2\pi_{AB}$ due to the fact that edge-to-face phenyl attraction stabilizes the structure by about 2.2 kcal/mol.[25] In our case, the phenyl–phenyl distance in $\mathbf{3}_2\pi_{AB}$ is longer than in ref 25, so the interaction energy should be less. Comparing the interaction energy of $\mathbf{1}_2\pi$, to that of $\mathbf{3}_2\pi_{AB}$ provides some insights into the role of the bulky side groups that can provide additional stabilization.[26] In this case we find that the latter is larger by 10.49 kcal/mol due to the stabilization effects of the side groups. Assuming a simple additivity approximation, this difference could be accounted for by the six edge-to-face phenyl–phenyl interactions each contributing ∼1.7 kcal/mol. This estimated value of a phenyl–phenyl vdW attraction is consistent with ref 25. Isomers $\mathbf{3}_2\pi_{AB}$ and $\mathbf{3}_2(RR2)$ are only ∼2.5 kcal/mol apart, so there is a good chance for these two

dx.doi.org/10.1021/ja509243p | J. Am. Chem. Soc. 2014, 136, 18009–18022

Table 7. E_{int} and Selected Distances of the Optimized Dimers of 3 Using (U)M05-2X/6-31G(d,p), Compared with XRD Data[a]

	$3_2(RR1)$	$3_2(RR2)$	$3_2(RR3)$	$3_2(RS1)$	$3_2(RS2)$	$3_2\pi_{PB}$[b]	$3_2\pi_{AB}$
E_{int}(before ZPE)	−17.01	−25.23	−21.39	−14.64	−23.37	−16.22	−21.20
E_{int}(ZPE corr)	3.52	3.75	3.66	3.38	3.75	1.97	2.55
E_{int}(after ZPE)	−13.49	−21.48	−17.73	−11.27	−19.62	−14.25	−18.65
symmetry	C_2	C_2	C_2	S_2	none	D_3	S_6
r	1.604	1.618	1.598	1.599	1.600	3.106	2.936
r(XRD)[c]							3.017
D_{cc}						3.142	3.066
D_{cc}(XRD)[c]							3.111
spin density[d]	0	0	0	0	0	0.656	0

[a] E_{int} values are in kcal/mol and distances are in Å. [b] Geometry is not fully converged. [c] For the XRD data at 100 K, see the CIF files in the Supporting Information. [d] Sum of Mulliken spin density of a monomer in the dimer.

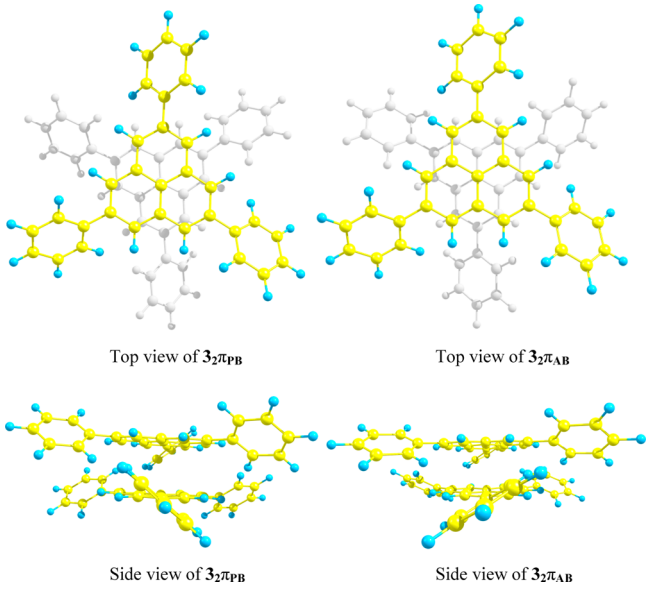

Figure 9. Top/side view of the two 3_2 π-dimers. PB indicates parablade and AB indicates antiblade configurations.

isomers to coexist. Solvent as well as temperature could be influential in determining the preferred structure.

We actually prepared **3** in eight steps from 2,7-diphenylnaphthalene. Recrystallization from a toluene−hexane solution gave dark violet cubic crystals. X-ray crystallographic analysis of the single crystal revealed that **3** adapts a π-dimer form with extraordinary short separation distance, r, between the α-carbons (3.017 Å at 100 K and 3.067 Å at 300 K). Figure 10 shows the crystal structure of 3_2 π-dimer determined at 100 K.

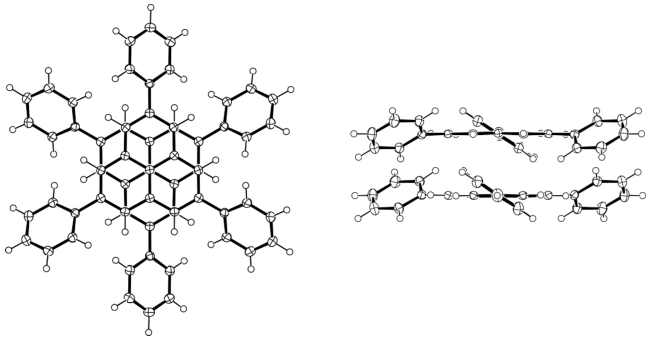

Figure 10. ORTEP drawings of 3_2 π-dimer: (left) top view and (right) side view.

The central carbon−carbon distance, D_{cc}, is 3.111 Å at 100 K and 3.145 Å at 300 K, which are longer than the α-carbon distances. Thus 3_2 π-dimer forms concave-concave overlap in solid state, in contrast to convex-convex overlap of 6_2 π-dimer (r = av. 3.306 Å and D_{cc} = 3.201 Å, at 300 K).[1a] This difference in the overlap motif arises from smaller steric repulsion of phenyl groups compared to *tert*-butyl groups. Phenyl groups in the 3_2 π-dimer adopt edge-to-face configuration, and therefore, **3** prefers the 3_2 π-antiblade ($3_2\pi_{AB}$) form over the 3_2 π-parablade ($3_2\pi_{PB}$) form in solid state. All these experimental findings are fully consistent with the computational results.

A toluene solution of 3_2 π-dimer at room temperature showed a well-resolved multiline ESR spectrum corresponding to monomeric **3** (Figure 11a,b). The hyperfine coupling constant (HFCC) of the phenalenyl α-proton was determined to be 0.620 mT, which is identical to those of parent phenalenyl (0.63 mT) and **6** (0.62 mT), indicating that an unpaired electron mostly resides on the phenalenyl moiety. The ESR signals of **3** decreased in the intensity with decreasing temperature and almost disappeared at 170 K. The drop in signal intensity is assignable to the formation of a diamagnetic dimer. The enthalpy and entropy changes for the dimerization were determined to be −9.6 kcal/mol and −18 eu, respectively, by variable-temperature ESR measurements (Figure 11d,e). In order to clarify the structure of dimeric species, we measured variable-temperature ^{1}H NMR spectra of **3** in CD_2Cl_2 (Figure 12a). The solution of **3** gave no signal at 273 K, whereas at 223 K ring protons appeared as two broad signals at 7.5 and 6.8 ppm and upon cooling progressive line sharpening was observed. Considering that similar behavior is observed for the π-dimerization of **6**, **3** would prefer π-dimer form over σ-dimer also in solution state. Good agreement between the observed and calculated chemical shifts (H_o, 7.4 ppm; H_m, 7.1 ppm; H_p, 7.1 ppm; H_{PLY}, 6.3 ppm; GIAO-HF/6-311+G**) supports the formation of the π-dimer. We did not obtain any evidence of σ-dimerization for **3** by the ^{1}H NMR studies.

Shorter π−π contact of 3_2 π-dimer than 6_2 π-dimer leads to wider HOMO−LUMO splitting that is formed by bonding and antibonding combinations of two SOMOs. Solid 3_2 π-dimer in a KBr pellet showed an intense broad band centered at 574 nm (Figure 12b), which is blue-shifted with respect to the band of 6_2 π-dimer (613 nm).

Tris(perfluorophenyl)-Phenalenyl (TPFPPLY). The perfluorophenyl analogue of **3** is TPFPPLY (**4**). Experimental data were published recently by Kubo's group.[27] In ref 27, two association modes were found: $4_2(RR3)$ and 1D stacking. We have addressed only possible dimer structures here and obtained five 4_2 σ-dimers and two 4_2 π-dimers. Optimized

dx.doi.org/10.1021/ja509243p | J. Am. Chem. Soc. 2014, 136, 18009−18022

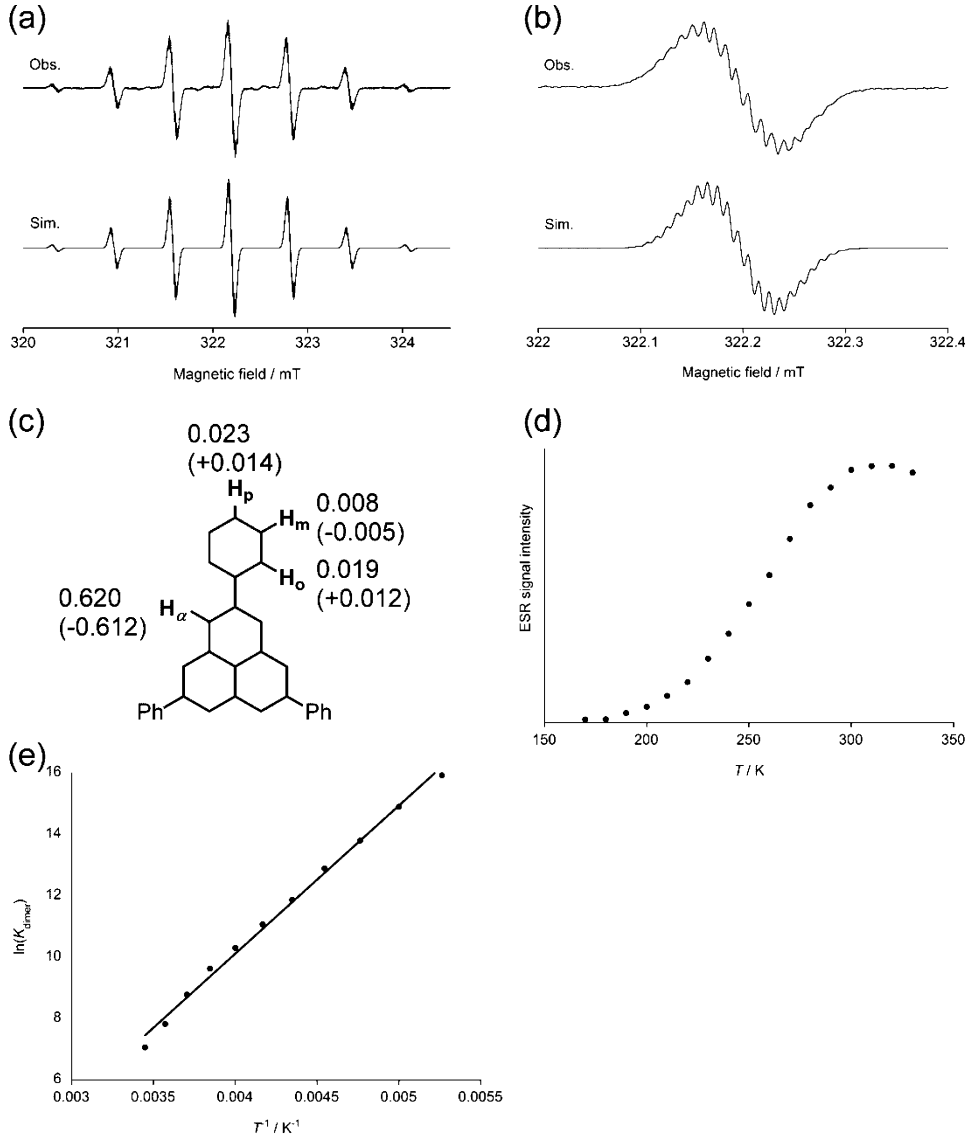

Figure 11. (a) Observed (1×10^{-5} M, g = 2.003) and simulated ESR spectra of **3** in toluene at 270 K. (b) Magnified view of the central peak. (c) Determined HFCCs (in mT) of **3**. In parentheses, HFCCs estimated with a UBLYP/6-31G**//UB3LYP/6-31G** method and the McConnell model (Q = −2.4 mT). (d) Temperature dependence of ESR signal intensity of **3**. (e) Temperature dependence of the dimerization constant K_{dimer} of **3**.

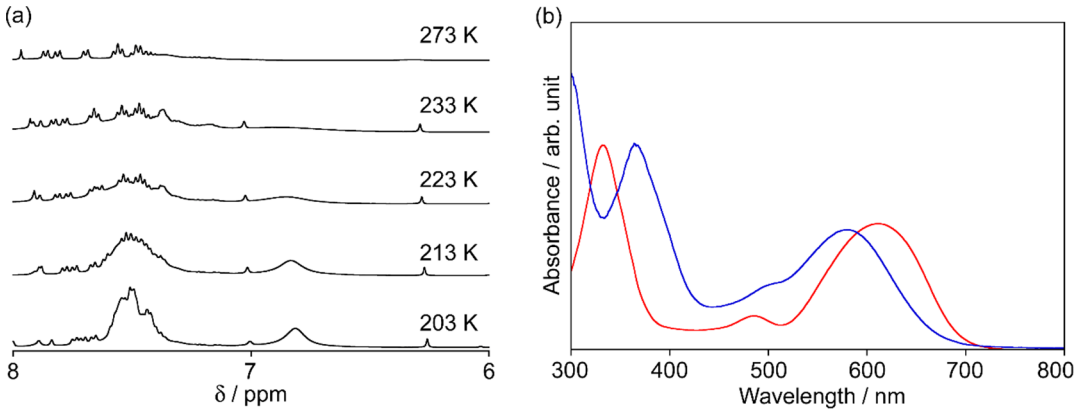

Figure 12. (a) Variable-temperature ^{1}H NMR spectra of **3** (10 mM) in CD_2Cl_2. Broad peaks around 7.5 ppm and 6.8 ppm are assignable to phenyl and phenalenyl protons, respectively. Small sharp peaks at 8 to 7.5 ppm are derived from 2,5,8-triphenylphenalenone. (b) UV−vis spectra of (blue line) $\mathbf{3}_2$ π-dimer and (red) $\mathbf{6}_2$ π-dimer in a KBr pellet at room temperature.

dx.doi.org/10.1021/ja509243p | J. Am. Chem. Soc. 2014, 136, 18009−18022

geometries as well as E_{int} of these $\mathbf{4}_2$-dimers are shown in Figure 13 and Table 8.

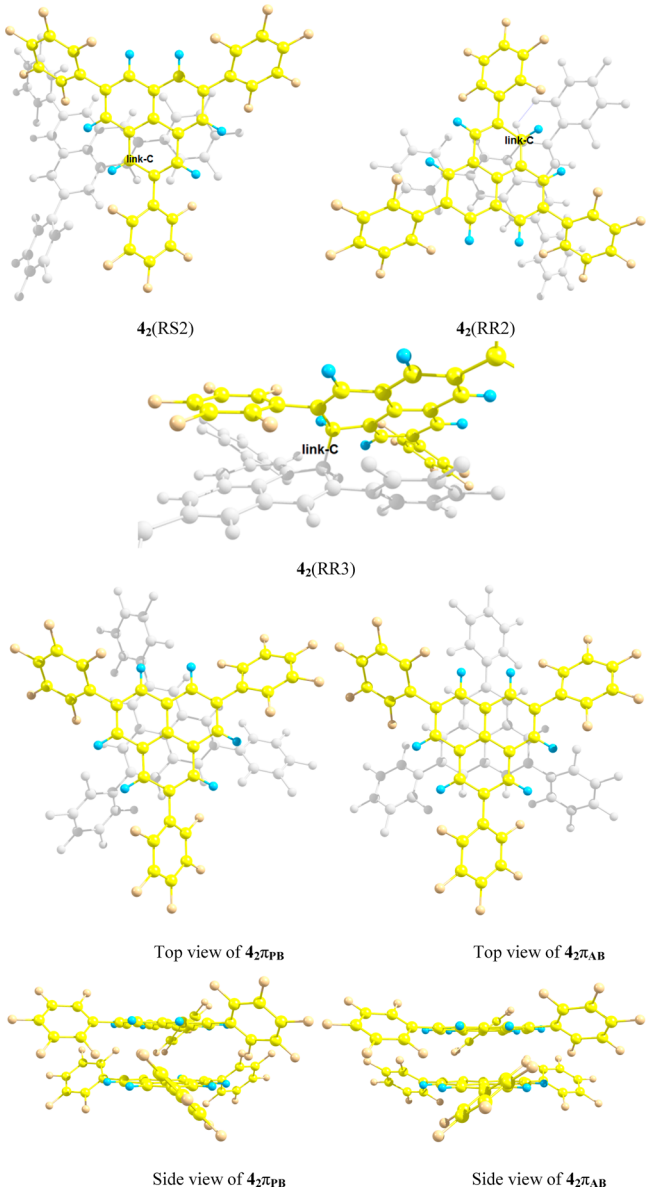

Figure 13. Top/side views of optimized geometries of five low-energy $\mathbf{4}_2$-dimers. The other two are given in Figure S7.

According to Table 8, the predicted structure with the lowest energy is a σ-bonded dimer $\mathbf{4}_2(RR3)$. $\mathbf{4}_2(RR3)$ is one of the two association modes discussed in ref 27. Unlike **3**, the *RR*3 configuration is slightly more stable than *RR*2 but they are both much more stable than the other $\mathbf{4}_2$-dimers. We attribute this additional stabilization to the increased stabilization by substitution of fluorine over hydrogen in the phenyl groups providing a perfluorophenyl−phenalenyl attraction that is stronger than that of central phenalenyl−phenalenyl attraction in $\mathbf{4}_2(RR3)$, as this stabilization appears to be analogous to the well-known phenyl−perfluorophenyl stabilizing effect.[28] The energy of second most stable structure, $\mathbf{4}_2(RR2)$, is by ∼2 kcal/mol higher than that of $\mathbf{4}_2(RR3)$. This small energy difference makes it possible for these two $\mathbf{4}_2$ σ-dimers to coexist. The other three $\mathbf{4}_2$ σ-dimers are 8∼10 kcal/mol higher than $\mathbf{4}_2(RR3)$. The optimization of $\mathbf{4}_2\pi_{PB}$ is not fully converged due to the same reasons as in the $\mathbf{3}_2\pi_{PB}$ case but the energy of $\mathbf{4}_2\pi_{PB}$ did not change over a wide range of geometry iterations on a rather flat PES. The energy of $\mathbf{4}_2\pi_{PB}$ obtained in this manner is very close to that of $\mathbf{4}_2\pi_{AB}$. Stronger phenyl−phenyl π−π repulsion occurs in $\mathbf{4}_2\pi_{PB}$ than in $\mathbf{3}_2\pi_{PB}$ and this leads to a significant distortion from the ideal D_3 symmetry whereby the torsional angle around the central CC contact deviates from the ideal[11] 0° or 60° for the parent compound $\mathbf{1}_2$ and becomes 44°. This distortion reduces the steric repulsion among the phenyl groups but also reduces the pancake bonding between the two phenalenyls. The result is that the pancake bonded $\mathbf{4}_2\pi$ configuration is overall less stable than the $\mathbf{4}_2$ σ-dimers. The large value of the spin density in this case also indicates that this configuration provides little SOMO-SOMO pancake-bonding interaction. It is interesting to note that neither of the $\mathbf{4}_2$ π-dimers has been observed.

Trimethyl-Phenalenyl (TMPLY). The next system we studied is the trimethyl-phenalenyl (TMPLY, **5**), which has been recently synthesized and characterized. These results are provided here and analyzed in terms of the computational modeling. Optimized geometries and relevant data for the $\mathbf{5}_2$-dimers are shown in Figure 14 and Table 9.

Table 9 summarizes the computed data for various tautomers of $\mathbf{5}_2$-dimers. The most stable is the $\mathbf{5}_2$ σ-dimer $\mathbf{5}_2(RR2)$ while $\mathbf{5}_2(RR3)$ and $\mathbf{5}_2(RS2)$ are also competitive with ∼1 kcal/mol higher in energy. The π-dimer $\mathbf{5}_2\pi$ is less stable than all $\mathbf{5}_2$ σ-dimers. Before ZPE correction, the energy difference between $\mathbf{5}_2$ π-dimers and $\mathbf{5}_2$ σ-dimers is in the 3−6 kcal/mol range. However the ZPE correction narrows down this energy difference to 0.6−3.6 kcal/mol. Based upon the E_{int} in Table 9, $\mathbf{5}_2(RR2)$ would be most preferred but the other $\mathbf{5}_2$-dimers including $\mathbf{5}_2\pi$ might be also generated due to the small computed energy difference. Dependent on the solvent some of these $\mathbf{5}_2$-dimers could coexist. In order to further explore the possibility of molecular fluctuation, the bond stretching scan

Table 8. E_{int} and Selected Distances of the Optimized $\mathbf{4}_2$-Dimers Using (U)M05-2X/6-31G(d,p)[a]

	$\mathbf{4}_2(RR1)$	$\mathbf{4}_2(RR2)$	$\mathbf{4}_2(RR3)$	$\mathbf{4}_2(RS1)$	$\mathbf{4}_2(RS2)$	$\mathbf{4}_2\pi_{PB}$[b]	$\mathbf{4}_2\pi_{AB}$
E_{int}(before ZPE)	−22.79	−32.36	−33.43	−24.59	−28.32	−20.86	−21.31
E_{int}(ZPE corr)	4.52	5.04	4.32	4.69	4.54	NA	2.39
E_{int}(after ZPE)	−18.27	−27.32	−29.15	−19.90	−23.78	NA	−18.91
symmetry	C_2	C_2	C_2	S_2	none	D_3	S_6
r	1.605	1.616	1.590	1.594	1.602	3.414[c]	3.100
D_{cc}						3.383	3.141
spin density[d]	0	0	0	0	0	0.937	0.684

[a] E_{int} values are in kcal/mol and distances are in Å. [b] Geometry is not fully converged. [c] Large value due to significant distortion from D_3 symmetry. [d] Sum of Mulliken spin density of a monomer in the dimer.

dx.doi.org/10.1021/ja509243p | J. Am. Chem. Soc. 2014, 136, 18009−18022

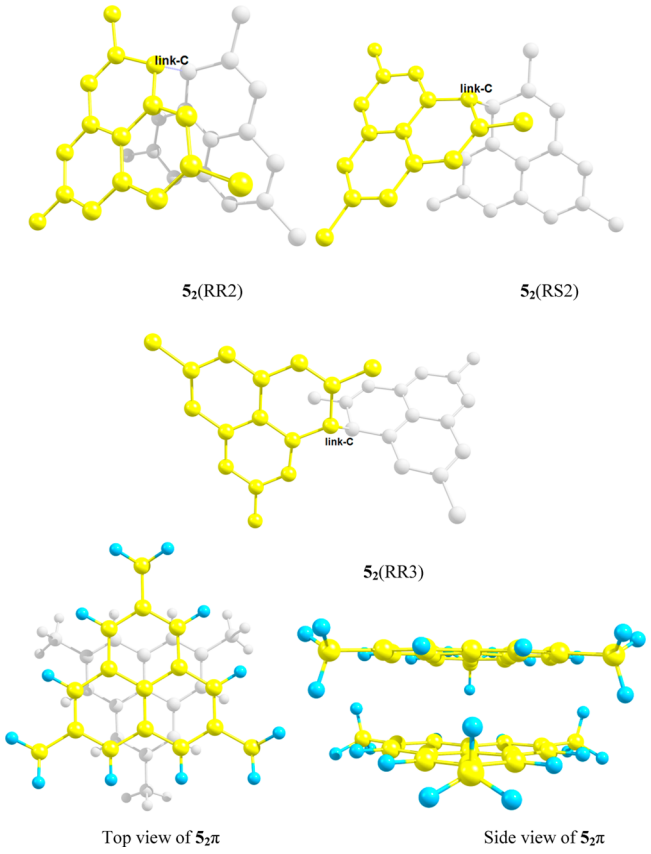

Figure 14. Top/side views of four low-energy 5_2-dimers. Hydrogen atoms are omitted for clarity for the 5_2 σ-dimers. The other two are given in Figure S8.

along the transition between $5_2(RR2)$ and $5_2\pi$ is presented in Figure 15 and Table 10.

According to Figure 15 and Table 10, dissociation behavior between $5_2(RR2)$ and $5_2\pi$ is very similar to the scans of 1_2 and 2_2. It is noteworthy that the barrier, $\Delta E_{TS,}$ along this scan is only 3.50 kcal/mol, which is ~2 kcal/mol smaller than that for the parent system, 1_2 (5.10 kcal/mol) or for the perfluorinated case, 2_2 (5.69 kcal/mol). This small value indicates that molecular transformation between $5_2(RR2)$ and $5_2\pi$ is more likely to happen and the chance of coexistence of 5_2 σ-dimers and $5_2\pi$ is significant. Again, the large difference between the relaxed and parallel rigid scan indicates that the 5_2 π-dimer formation is asynchronous.

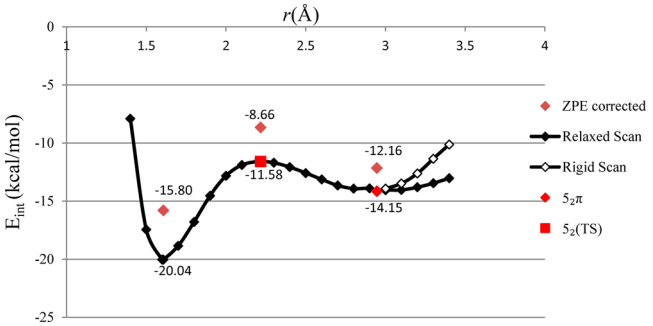

Figure 15. Dissociation scan along $5_2(RR2)$ and $5_2\pi$. Energy calculated at the UM052X/6-31G(d,p) level.

Table 10. Energies and Distances for Stationary Points on the $5_2(RR2)$–$5_2\pi$ Scan[a]

	$5_2(RR2)$	5_2(TS)	$5_2\pi$
E_{int}(before ZPE)	−20.04	−11.58	−14.15
E_{int}(ZPE corr)	4.24	2.92	1.99
E_{int}(after ZPE)	−15.80	−8.66	−12.16
r	1.607	2.217	2.950
ΔE_{TS}		3.50	

[a]Energy values are in kcal/mol and distances are in Å.

We describe the synthesis of **5** in the Methods section. The reaction produced a highly colored (pink-violet) solution, which indicates the generation of **5** or 5_2-dimers; however, the concentration of the solution afforded colorless platelet crystals. X-ray crystallographic analysis revealed that **5** adopts a σ-dimer form in the colorless solid state and its configuration is very close to the most stable σ-form, $5_2(RR2)$, as shown in Figure 16. Heating at 573 K of 5_2 σ-dimer plates in a sealed degassed tube resulted in melting accompanied by a color change from colorless to purple, and subsequent cooling the purple liquid gave purple plates together with colorless 5_2 σ-dimer plates. X-ray crystallographic analysis of the purple plate at 100 K revealed that the purple state is a π-dimer form (Figure 16) with a short contact of α-carbons (r = av. 3.054 Å) and relatively long D_{cc} (3.145 Å). Thus, **5** can exist in both σ- and π-dimer forms in the solid state, and this facile change from $5_2(RR2)$ to $5_2\pi$ is in agreement with our computational predictions.

Dissolution of 5_2 σ-dimer in toluene gave a well-resolved multiline ESR spectrum corresponding to monomeric **5** (Figure 17a). The HFCC of the phenalenyl α-proton was determined

Table 9. Interaction Energies, E_{int}, and Selected Distances of the Optimized the 5_2-Dimers Using (U)M05-2X/6-31G(d,p), Compared with XRD Data[a]

	$5_2(RR1)$	$5_2(RR2)$	$5_2(RR3)$	$5_2(RS1)$	$5_2(RS2)$	$5_2\pi$
E_{int}(before ZPE)	−18.76	−20.04	−19.24	−17.11	−18.94	−14.15
E_{int}(ZPE corr)	5.50	4.24	4.64	4.35	4.35	1.99
E_{int}(after ZPE)	−13.26	−15.80	−14.60	−12.76	−14.59	−12.16
symmetry	C_2	C_2	C_2	S_2	none	D_{3d}
r	1.610	1.607	1.586	1.601	1.596	2.950
r(XRD)[b]		1.614				3.053
D_{cc}						3.061
D_{cc}(XRD)						3.145
spin density[c]	0	0	0	0	0	0

[a]E_{int} values are in kcal/mol and distances are in Å. Note: a very small imaginary frequency on $5_2\pi$ was seen and corrected. [b]For XRD data see the CIF files in the Supporting Information. r(XRD) is an average [c]Sum of Mulliken spin density of a monomer in the dimer.

dx.doi.org/10.1021/ja509243p | J. Am. Chem. Soc. 2014, 136, 18009−18022

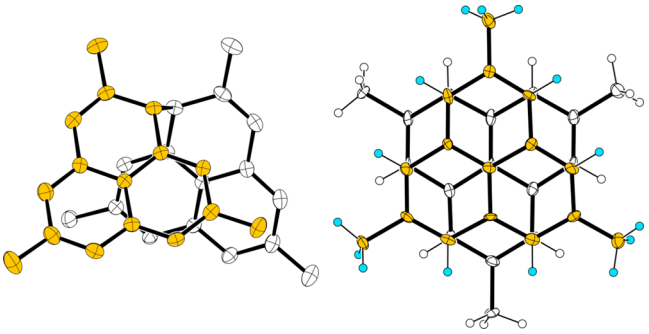

Figure 16. ORTEP drawings of (left) $\mathbf{5}_2$ σ-dimer and (right) $\mathbf{5}_2$ π-dimer. Hydrogen atoms of $\mathbf{5}_2$ σ-dimer are omitted for clarity.

to be 0.620 mT. Upon cooling, the ESR signals decreased in intensity and almost disappeared at 170 K, due to dimerization. The enthalpy and entropy changes for the dimerization were determined to be −9.7 kcal/mol and −22 eu, respectively, by variable-temperature ESR measurements (Figure 17c,d). The structure of diamagnetic species at low temperature is uncertain, because solution ^{1}H NMR measurement at 173 K gave a complicated spectrum (not shown).[29] Many isomers of the $\mathbf{5}_2$ dimer might exist in the solution state, as predicted by the presented quantum chemical calculations.

Tri-*tert*-butyl-Phenalenyl (TBPLY). In the crystal structure, TBPLY forms π-dimers in the staggered configuration avoiding steric repulsion.[1a] Five σ-dimers and a π-dimer have been identified in the presented modeling. Figure 18 shows the structures; Table 11 lists the key parameters.

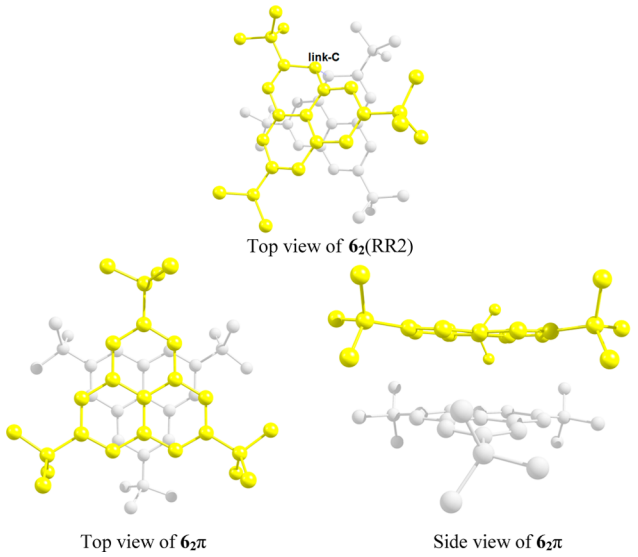

Figure 18. Top/side views of the two low-energy $\mathbf{6}_2$-dimers. Hydrogen atoms are omitted for clarity.

The most stable $\mathbf{6}_2$-dimer is $\mathbf{6}_2(RR2)$ with an E_{int} of −12.33 kcal/mol. The other four $\mathbf{6}_2$ σ-dimers are significantly less stable. The small E_{int} for the five $\mathbf{6}_2$ σ-dimers (besides $\mathbf{6}_2(RR2)$) are mainly due to steric repulsion. *tert*-butyl (TB) is a bulky and both TB−TB repulsion and TB−phenalenyl repulsion increase the energy significantly for all $\mathbf{6}_2$ σ-dimers except $\mathbf{6}_2(RR2)$. In the $\mathbf{6}_2(RR2)$, on the other hand, the TB groups are oriented in a staggered fashion avoiding each other quite well. The E_{int} for

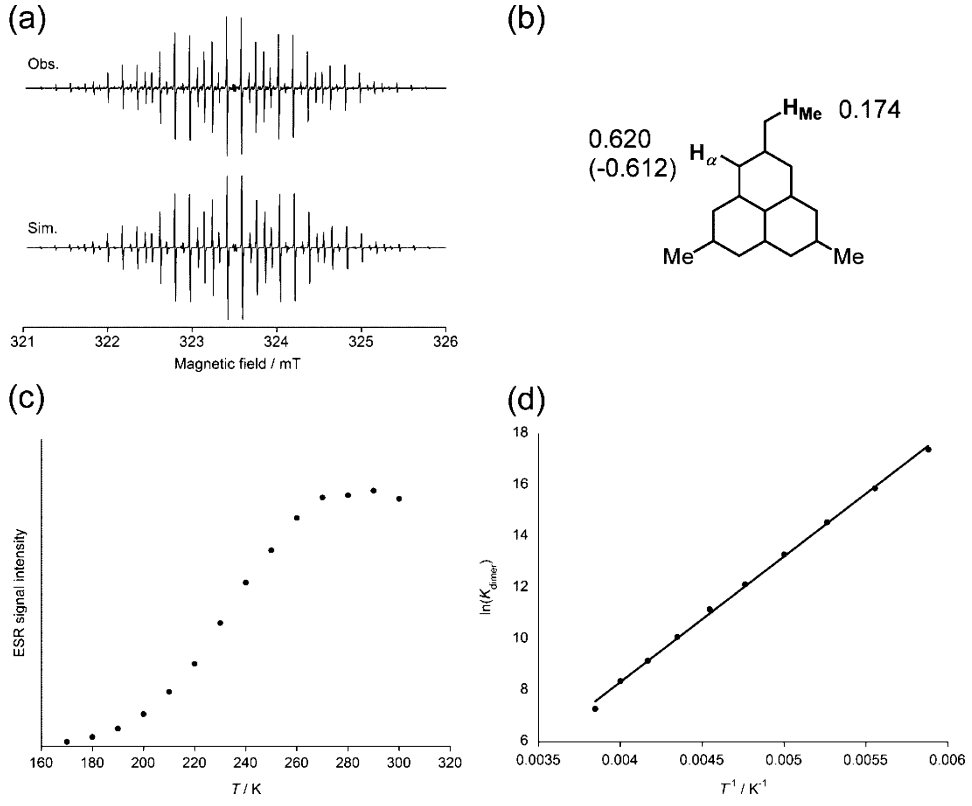

Figure 17. (a) Observed (1×10^{-5} M, g = 2.003) and simulated ESR spectra of **5** in toluene at 250 K. (b) Determined HFCCs (in mT) of **5**. In parentheses, HFCCs estimated with a UBLYP/6-31G**//UB3LYP/6-31G** method and the McConnell model (Q = −2.4 mT). (c) Temperature dependency of ESR signal intensity of **5**. (d) Temperature dependence of the dimerization constant K_{dimer} of **5**.

dx.doi.org/10.1021/ja509243p | J. Am. Chem. Soc. 2014, 136, 18009−18022

Table 11. Interaction Energies, E_{int}, and Selected Distances of the Optimized 6_2-Dimers Using (U)M05-2X/6-31G(d,p)[a]

	$6_2(RR1)$	$6_2(RR2)$	$6_2(RR3)$	$6_2(RS1)$	$6_2(RS2)$	$6_2\pi$[b]
E_{int}(before ZPE)	−9.16	−16.08	−8.12	−9.32	−10.94	−12.17
E_{int}(ZPE corr)	3.93	3.75	4.34	3.72	4.00	0.70
E_{int}(after ZPE)	−5.23	−12.33	−3.78	−5.60	−6.94	−11.47
symmetry	C_2	none	C_2	S_2	none	S_2
r	1.601	1.637	1.618	1.598	1.615	3.298
r(XRD)[c]						3.306
D_{cc}						3.209
D_{cc}(XRD)[c]						3.201
spin density[d]	0	0	0	0	0	0.794

[a] E_{int} values are in kcal/mol and distances are in Å. [b] Calculation geometry adopted from ref 14. [c] Values from refs 1a and 23. [d] Sum of Mulliken spin density of a monomer in the dimer.

Table 12. Comparison of Computed Parameters for π-Stacking Phenalenyl Derivative Dimers[a]

	$1_2\pi$	$2_2\pi$	$3_2\pi_{AB}$	$4_2\pi_{AB}$	$5_2\pi$	$6_2\pi$[f]	3F-PLY$_2\pi$[g]	6F-PLY$_2\pi$[g]	3CN-PLY$_2\pi$[f,g]	6CN-PLY$_2$[f,g]	3NO$_2$-PLY$_2$[f,g]	3NH$_2$-PLY$_2$[f,g]
E_{int}(before ZPE)	−10.71	−15.32	−21.20	−21.31	−14.15	−12.16	−14.58	−17.21	−16.71	−12.95	−15.45	−17.55
E_{int}(ZPE corr)	1.47	1.94	2.55	2.39	1.99	0.69	2.36	1.41	1.85	0.91	1.61	3.77
E_{int}(after ZPE)	−9.24	−13.38	−18.65	−18.91	−12.16	−11.47	−12.22	−15.80	−14.86	−12.04	−13.84	−13.78
$E_{SOMO-SOMO}$	−13.56	−5.72	−21.99	−2.64	−21.50	−7.54	−22.61	−8.66	−18.80	−5.89	−22.94	−24.45
symmetry	D_{3h}	D_{3h}	S_6	S_6	D_{3d}	S_2	D_{3d}	D_{3d}	D_{3d}	D_{3d}	D_{3d}	D_{3d}
r	3.084	2.933	2.936	3.100	2.950	3.298	2.920	2.992	2.967	3.209	2.894	2.890
D_{cc}	3.137	3.109	3.066	3.141	3.061	3.209	3.095	3.118	3.091	3.256	3.048	3.109
spin density[b]	0.642	0.702	0	0.684	0	0.794	0	0.625	0.446	0.825	0.049	0
α-C spin density[c]	0.215	0.208	0	0.312	0	0.269	0	0.226	0.155	0.232	0.017	0
α-C charge[d]	−0.218	0.253	−0.194	−0.136	−0.194	−0.184	−0.306	0.336	−0.146	0.023	−0.163	−0.191
CF point[e]	2.70	2.50	2.936	2.950								

[a] E_{int} values are in kcal/mol and distances are in Å. [b] Sum of Mulliken spin density of a monomer in the dimer. [c] Average Mulliken spin density for π-carbons in phenalenyl. [d] Average Mulliken charge on α-carbon. [e] Coulson−Fischer point from rigid (for **1** and **2**) and relaxed (**3** and **5**) scans. [f] Values from ref 15. [g] 3F-PLY$_2\pi$ refers to 3β-trifluoro-phenalenyl and 6F-PLY$_2\pi$ refers to 6α-hexafluoro-phenalenyl. (Structural formulas for 3F-PLY$_2\pi$, 6F-PLY$_2\pi$, 3CN-PLY$_2\pi$, 3NO$_2$-PLY$_2\pi$, 3NH$_2$-PLY$_2\pi$, and 6CN-PLY$_2\pi$ are shown in Scheme S2.)

$6_2\pi$ is −11.47 kcal/mol and is very close to that of $6_2(RR2)$. As we mentioned above, only $6_2\pi$ was observed and characterized for TBPLY dimers, however the coexistence of *RR2* and π dimer in a very similar molecule, tri-*tert*-butyl-1,3-diazaphenalenyl, has been found and studied.[14,30] The reason why no 6_2 σ-dimers have been observed could be that specific solution environments can stabilize the pancake bonded $6_2\pi$ dimer over the σ-dimers. Moreover, the barrier between $6_2\pi$ and $6_2(RR2)$ may be high preventing the transformation from $6_2\pi$ to $6_2(RR2)$ to occur.

Trends in Pancake Bonds. Next we discuss the different pancake bonded π-dimers and their strength, geometry, and spin densities as a function of substitution.

In order to find the relations and insights for π-dimerization, we compare in Table 12 all π-dimers, including the six mentioned above, and two more fluoro-substituted systems and some our previously studied molecules that are closely related to this series.[15]

Figure 19 shows that the $E_{SOMO-SOMO}$ has a strong relationship with the computed spin density using either the α-carbon or the total monomer spin density. Note that the limiting value obtained from the correlation indicates that π-dimers with larger spin density have less π−π bonding and are mixtures of singlet and triplet states in the electron configuration, in which $E_{SOMO-SOMO}$ is small. In an extreme case where $E_{SOMO-SOMO}$ goes to 0 kcal/mol, we have two completely separated phenalenyl radicals. Small spin density, however, indicates stronger π−π bonding, thus resulting in purer singlet-state form and large $E_{SOMO-SOMO}$.

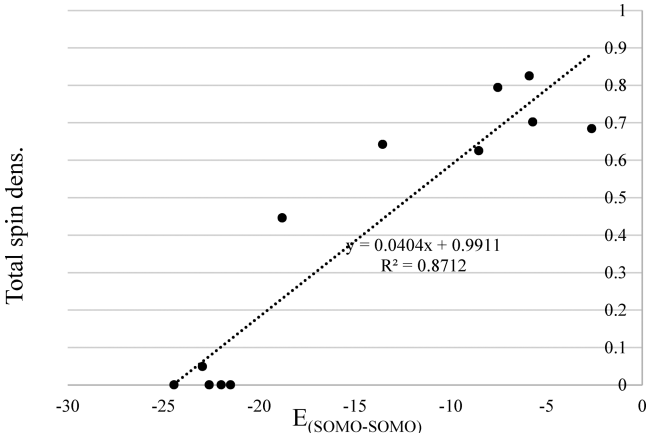

Figure 19. $E_{SOMO-SOMO}$ (in kcal/mol) vs total monomer spin density (in |e|) for π-dimers of PLY-derivatives in Table 12.

At the given level of theory all six systems prefer σ-dimers over π-dimers based on their interaction energies (Table 13). However, the energy differences between the most stable σ- and π-dimer fall into three groups. For the 2_2- and 4_2-dimers the σ-dimer is much more stable than π-dimer (by ∼9−11 kcal/mol) indicating the σ-dimer is the most likely dimerization mode in crystals as well as in solutions. For 1_2-, 3_2-, 5_2-dimers, the differences between σ- and π-dimer become smaller (by ∼3−4 kcal/mol) where coexistence of these dimer is more possible. For 6_2-dimer, these two dimers are almost the same in

dx.doi.org/10.1021/ja509243p | J. Am. Chem. Soc. 2014, 136, 18009−18022

Table 13. Summary of the Preferred Configurations for Phenalenyl-Based Dimers As Predicted by (U)M05-2X/6-31G(d,p); ZPE-Corrected Values Are Listed

monomer	$E_{int}(\pi) - E_{int}(\sigma)$ [kcal/mol][a]
1, PLY	3.6[b]
2, PFPLY	8.8
3, TPPLY	2.8
4, TPFPPPLY	10.8
5, TMPLY	3.64
6, TBPLY	0.86

[a]The lowest energy σ- and π-dimers are compared. [b](U)M05-2X/6-31G(d).

energy so the coexistence and molecular fluctuation of σ- and π-dimer are very likely to happen and solvent effect may play a significant role in determining the configuration of the dimer.

CONCLUDING COMMENTS

A series of substituted phenalenyl dimers have been investigated. The main points are summarized below.

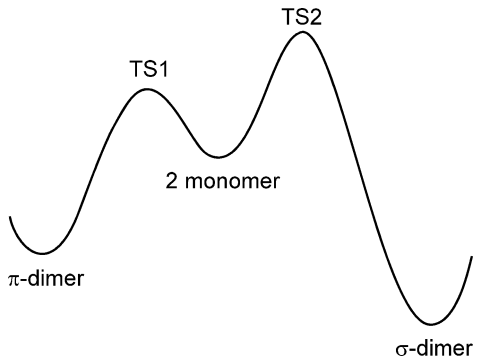

Figure 20. Schematic illustration of barriers separating the σ- and π-dimers from the two isolated monomer radicals.

1. π-Dimer formation can proceed through two pathways that we identified in this work. One is a direct formation from two radical monomers. In that case, there is no or very low barrier between the monomers and the π-dimer, but the formation of six $\alpha-\alpha$ contacts is not equivalent, one of them is shorter than the other five during the approach. Therefore, the direct pathway is concerted and asynchronous. The other pathway proceeds from two monomers to a σ-dimer (*RR* or *SS*) and then via a higher barrier path to a π-dimer, that is, via a stepwise mechanism. Since *RS* σ-dimers lead to eclipsed π-dimers, which are less stable than a staggered π-dimer, only chiral (*RR* or *SS*) σ-forms are viable intermediates on the path from monomers to π-dimers. For the tri-*tert*-butyl (**6**) derivative, that pathway is prohibited by steric reasons.

2. Strength of the π-stacking pancake interaction depends strongly on substituents. This is reflected in the wide range of SOMO−SOMO bonding energy values and spin densities as obtained by UDFT.

3. Many σ-dimer configurations compete some of which are separated by small barriers leading to fluxional structures between σ-bonded configurations or σ- and π-bonded configurations.

4. The relative energies of the various σ-bonded configurations depend strongly on the substituents and reflect a range of group−group interactions, such as phenyl−phenyl, phenyl−perfluorophenyl, phenyl−phenalenyl, etc. interactions. The same effects are further modulated when π-stacking pancake interactions are present.

5. The presented computations do not include solvent effects and crystal packing effects, which can substantially alter the preferred configurations. The dimerization mode may show differences in the solid state and in solution phases because of the intermolecular interactions. A well-studied case indicating these complexities is represented by the crystal structure of perchloro-phenalenyl (PCPLY).[31] In that case the phenalenyl part of the radical is strongly distorted from planarity yielding a ruffled edge which aggregate into 1D columns in the crystal. Pancake bonding and dimerization are prevented by the large vdW radius of chlorine. It sounds plausible to us—as one of the reviewers opined—that solid-state effects over-ride σ-dimerization by affording a more efficient packing of the π-dimers in this case.[31]

6. Although the computations demonstrate that all phenalenyls treated in this paper energetically prefer σ-dimer forms over π-dimer forms, it might be possible that only π-dimer is observed, in case of that E(TS1) is much lower than E(TS2), as shown in Figure 20. We have shown that for **1** and **2** there is no TS1 and the formation of the π-dimer can proceed without a barrier from the two monomers. In other cases structural changes induced by aggregation from monomer to the π-dimer might increase E(TS1). However, these structural changes are small for **3** and **4** as illustrated by the torsional angles in Table 14 showing that the change in the phenyl-to-phenalenyl torsion is modest, less than 10° in all four π-dimers compared to the respective monomers. This indicates that the α-sites are not "protected" by these large substituents. It looks like there is a good special fit between the two monomers as they come together in the π-dimer for both **3** and **4**. The case of **5** and **6** is probably similar to that of **3** and **4**.

ASSOCIATED CONTENT

Supporting Information

Experimental and computational details, CIF files for crystal structures, absolute energies and Cartesian coordinates for all optimized structures, and a movie showing a σ- to π-dimer transformation. This material is available free of charge via the Internet at http://pubs.acs.org.

Table 14. Torsional Changes from Monomer to π-Dimers for 3 and 4 from the Optimized Geometries by (U)M05-2X/6-31G(d,p)

	3 (monomer)	$\mathbf{3}_2\pi_{PB}$	$\mathbf{3}_2\pi_{AB}$	**4** (monomer)	$\mathbf{4}_2\pi_{PB}$	$\mathbf{4}_2\pi_{AB}$
symmetry	D_3	D_3	S_6	D_3	D_3	S_6
phenyl-to-phenalenyl torsion	40.3°	39.6°	32.1° [a]	44.4°	46.3°	36.1°

[a]The XRD value at 100 K is 33.3° (average of two values).

dx.doi.org/10.1021/ja509243p | J. Am. Chem. Soc. 2014, 136, 18009−18022

AUTHOR INFORMATION

Corresponding Authors

kubo@chem.sci.osaka-u.ac.jp
kertesz@georgetown.edu

Notes

The authors declare no competing financial interest.

ACKNOWLEDGMENTS

We thank the U.S. National Science Foundation for its support of this research at Georgetown University (grant no. CHE-1006702). M.K. is member of the Georgetown Institute of Soft Matter. T.K. thanks JSPS for KAKENHI Grant No. 26288016.

REFERENCES

(1) (a) Goto, K.; Kubo, T.; Yamamoto, K.; Nakasuji, K.; Sato, K.; Shiomi, D.; Takui, T.; Kubota, M.; Kobayashi, T.; Yakushi, K.; Ouyang, J. *J. Am. Chem. Soc.* **1999**, *121*, 1619−1620. (b) Nakano, M.; Kubo, T.; Kamada, K.; Ohta, K.; Kishi, R.; Ohta, S.; Nakagawa, N.; Takahashi, H.; Furukawa, S.; Morita, Y.; Nakasuji, K. *Chem. Phys. Lett.* **2006**, *418*, 142−147. (c) Small, D.; Zaitsev, V.; Jung, Y.; Rosokha, S. V.; Head-Gordon, M.; Kochi, J. K. *J. Am. Chem. Soc.* **2004**, *126*, 13850−13858. (d) Lü, J.-M.; Roso kha, S. V.; Kochi, J. K. *J. Am. Chem. Soc.* **2003**, *125*, 12161. (e) Zaitsev, V.; Rosokha, S. V.; Head-Gordon, M.; Kochi, J. K. *J. Org. Chem.* **2006**, *71*, 520.

(2) (a) Hicks, R. G., Ed. *Stable Radicals: Fundamentals and Applied Aspects of Odd-Electron Compounds*; Wiley: Chichester, UK, 2010. (b) Morita, Y.; Suzuki, S.; Sato, K.; Takui, T. *Nature Chem.* **2011**, *3*, 197.

(3) (a) Del Sesto, R. E.; Miller, J. S.; Novoa, J. J.; Lafuente, P. *Chem. Eur. J.* **2002**, *8*, 4894. (b) Novoa, J. J.; Miller, J. S. *Acc. Chem. Res.* **2007**, *40*, 189.

(4) (a) Pal, S. K.; Itkis, M. E.; Tham, F. S.; Reed, R. W.; Oakley, R. T.; Haddon, R. C. *Science* **2005**, *309*, 281. (b) Kubo, T.; Shimizu, A.; Nakano, M.; Nakasuji, K. J. *Synth. Org. Chem. Jpn.* **2010**, *68*, 64. (c) Shimizu, A.; Nakano, M.; Hirao, Y.; Kubo, T. *J. Phys. Org. Chem.* **2011**, *24*, 876. (d) Haddon, R. C. *ChemPhysChem* **2012**, *13*, 3581. (e) Pal, S. K.; Bag, P.; Sarkar, A.; Chi, X. L.; Itkis, M. E.; Tham, F. S.; Donnadieu, B.; Haddon, R. C. *J. Am. Chem. Soc.* **2010**, *132*, 17258.

(5) (a) Mulliken, R. S.; Person, W. B. *Molecular Complexes*; Wiley & Sons: New York, 1969; Chap. 16. (b) Suzuki, S.; Morita, Y.; Fukui, K.; Sato, K.; Shiomi, D.; Takui, T.; Nakasuji, K. *J. Am. Chem. Soc.* **2006**, *128*, 2530.

(6) (a) Beneberu, H. Z.; Tian, Y.-H.; Kertesz, M. *Phys. Chem. Chem. Phys.* **2012**, *14*, 10713−10725. (b) Huang, J. S.; Sumpter, B. G.; Meunier, V.; Tian, Y.-H.; Kertesz, M. *Chem. Mater.* **2011**, *23*, 874−885. (c) Huang, J.; Kertesz, M. J. *J. Phys. Chem. A* **2007**, *111*, 6304−6315.

(7) (a) Reid, D. H. *Tetrahedron* **1958**, *3*, 339−352. (b) Gerson, F. *Helv. Chim. Acta* **1966**, *5*, 1463−1467. (c) Reid, D. H. *Chem. Ind.* **1956**, 1504. (d) Sogo, P. B.; Nakazaki, M.; Calvin, M. *J. Chem. Phys.* **1957**, *26*, 1343. (e) Paskovich, D. H.; Reddoch, A. H. *J. Am. Chem. Soc.* **1972**, *94*, 6938.

(8) Small, D.; Rosokha, S. V.; Kochi, J. K.; Head-Gordon, M. *J. Phys. Chem. A* **2005**, *109*, 11261−11267.

(9) Fourmigué, M. Organic π-Radicals in the Solid-State: From Localised to Delocalised σ-Bonding. In *The Importance of Pi-Interactions in Crystal Engineering-Frontiers in Crystal Engineering III*; Tiekink, E. R. T., Zukerman Schpector, J., Eds.; Wiley: Chichester, UK 2012; Chap. 6, pp 143−162.

(10) Devic, T.; Yuan, M.; Adams, J.; Fredrickson, D. C.; Lee, S.; Venkataraman, D. *J. Am. Chem. Soc.* **2005**, *127*, 14616.

(11) Cui, Z.-h.; Lischka, H.; Beneberu, H. Z.; Kertesz, M. *J. Am. Chem. Soc.* **2014**, *136*, 5539−5542.

(12) Wolinska-Mocydlarz, J.; Canonne, P.; Leitch, L. C. *Synthesis* **1974**, *1974*, 566−568.

(13) (a) Zhao, Y.; Schultz, N. E.; Truhlar, D. G. *J. Chem. Phys.* **2005**, *123*, 161103. (b) Zhao, Y.; Schultz, N. E.; Truhlar, D. G. *J. Chem. Theory Comput.* **2006**, *2*, 364−382.

(14) Tian, Y.-H.; Huang, J.; Kertesz, M. *Phys. Chem. Chem. Phys.* **2010**, *12*, 5084−5093.

(15) Tian, Y.-H.; Kertesz, M. *J. Am. Chem. Soc.* **2010**, *132*, 10648−10649.

(16) Mota, F.; Miller, J. S.; Novoa, J. J. *J. Am. Chem. Soc.* **2009**, *131*, 7699−7707.

(17) Cui, Z.-h.; Lischka, H.; Mueller, T.; Plasser, F.; Kertesz, M. *ChemPhysChem* **2014**, *15*, 165.

(18) Frisch, M. J.; et al. *Gaussian 09*, Revision D.01; Gaussian, Inc.: Wallingford, CT, 2013.

(19) Zhurko, G. A.; Zhurko, D. A. *Chemcraft*, Version 1.6, http://chemcraftprog.com.

(20) Grimme, S.; Schreiner, P. R. S. *Angew. Chem., Int. Ed.* **2011**, *50*, 12639−12642.

(21) (a) Morita, Y.; Aoki, T.; Fukui, K.; Nakazawa, S.; Tamaki, K.; Suzuki, S.; Fuyuhiro, A.; Yamamoto, K.; Sato, K.; Shiomi, D.; Naito, A.; Takui, T.; Nakasuji, K. *Angew. Chem., Int. Ed.* **2002**, *41*, 1793. (b) Morita, Y.; Miyazaki, E.; Kawai, J.; Sato, K.; Shiomi, D.; Takui, T.; Nakasuji, K. *Polyhedron* **2003**, *22*, 2219. (c) Morita, Y.; Suzuki, S.; Fukui, K.; Nakazawa, S.; Kitagawa, H.; Kishida, H.; Okamoto, H.; Naito, A.; Sekine, A.; Ohashi, Y; Shiro, M.; Sasaki, K.; Shiomi, D.; Sato, K.; Takui, T.; Nakasuji, K. *Nat. Mater.* **2008**, *7*, 48−51.

(22) McMillen, D. F.; Golden, D. M. *Annu. Rev. Phys. Chem.* **1982**, *33*, 493−532.

(23) (a) Fukui, K.; Sato, K.; Shiomi, D.; Takui, T.; Ito, K.; Kubo, T.; Goto, K.; Yamamoto, K.; Nakasuji, K.; Naito, A. *Mol. Cryst. Liq. Cryst.* **1999**, *334*, 49−58. (b) Fukui, K.; Sato, K.; Shiomi, D.; Takui, T.; Itoh, K.; Goto, K.; Kubo, T.; Yamamoto, K.; Nakasuji, K.; Naito, A. *Synth. Met.* **1999**, *103*, 2257−2258.

(24) (a) Jennings, W. B.; Farrell, B. M.; Malone, J. F. *Acc. Chem. Res.* **2001**, *34*, 885−894. (b) Wheeler, S. E.; Houk, K. N. *Mol. Phys.* **2009**, *107*, 749−760.

(25) Dance, I.; Scudder, M. *CrystEngComm* **2009**, *11*, 2233−2247.

(26) Schreiner, P. R.; Chernish, L. V.; Gunchenko, P. A.; Tikhonchuk, E. Y.; Hausmann, H.; Serafin, M.; Schlecht, S.; Dahl, J. E. P.; Carlson, R. M. K.; Fokin, A. A. *Nature* **2011**, *477*, 308−311.

(27) Uchida, K.; Hirao, Y.; Kurata, H.; Kubo, T.; Hatano, S; Inoue, K. *Chem. Asian J.* **2014**, *9*, 1823−1829.

(28) (a) Coates, G. W.; Dunn, A. R.; Henling, L. M.; Dougherty, D. A.; Grubbs, R. H. *Angew. Chem., Int. Ed. Engl.* **1997**, *36*, 248−251. (b) Coates, G. W.; Dunn, A. R.; Henling, L. M.; Ziller, J. W.; Lobkovsky, E. B.; Grubbs, R. H. *J. Am. Chem. Soc.* **1998**, *120*, 3641−3649.

(29) We temporally assigned the species observed at 173 K to two σ-dimers (*RR*/*SS* and *RS*) and one π-dimer. Further experiments will be necessary to confirm this assignment.

(30) Morita, Y.; Suzuki, S.; Fukui, K.; Nakazawa, S.; Kitagawa, H.; Kishida, H.; Okamoto, H.; Naito, A.; Sekine, A.; Ohashi, Y.; Shiro, M.; Sasaki, K.; Shiomi, D.; Sato, K.; Takui, T.; Nakasuji, K. *Nat. Mater.* **2008**, *7*, 48−51.

(31) (a) Koutentis, P. A.; Chen, Y.; Cao, Y.; Best, T. P.; Itkis, M. E.; Beer, L.; Oakley, R. T.; Brock, C. P.; Haddon, R. C. *J. Am. Chem. Soc.* **2001**, *123*, 3864. (b) Koutentis, P. A.; Haddon, R. C.; Oakley, R. T.; Cordes, A. W.; Brock, C. P. *Acta Crystallogr. B* **2001**, *57*, 680−691.